University of Nevada, Reno

Comparing Deformation at Soda Lake Geothermal Field from GPS and 3D Seismic

A thesis submitted in partial fulfillment of the
requirements for the degree of
Master of Science in Geophysics

by

Tyler Kent

Dr. John N. Louie, Thesis Advisor

Dr. Graham Kent, Thesis Advisor

May, 2013

UNIVERSITY OF NEVADA, RENO

THE GRADUATE SCHOOL

We recommend that the thesis

prepared under our supervision by

Tyler Kent

entitled

**Comparing Deformation at Soda Lake Geothermal Field from GPS and
3D Seismic**

be accepted in partial fulfillment of the

requirements for the degree of

MASTER OF SCIENCE

John N. Louie, Ph.D., Advisor

Graham Kent, Ph.D., Committee Member

Alan Fuchs, Ph.D., Graduate School Representative

Marsha H. Read, Ph.D., Associate Dean, Graduate School

May, 2013

Abstract

The transition between the two distinct structural regimes of the Walker Lane and the Basin and Range allows for complex transtensional fault interactions. The Carson Sink is the surface expression of the interaction of shear and extensional strains that cause both crustal extension and block rotation. This study investigates this tectonic shift at the Soda Lake geothermal field by comparing the direction and rate of deformation from both regional GPS and a 34 sq km 3D seismic survey. The GPS stations in the region estimate the strain field by comparing tensor solutions that show changing direction and magnitude of strain across the Carson Sink. Using stations surrounding the Soda Lake 3D seismic survey, the strain tensor produced is comparable in orientation to Basin and Range strain but has larger magnitudes. To quantify deformation within the Soda Lake 3D seismic survey, we calculate fault dip and offset of a deformed paleo-planer lacustrine mudstone. Plotting the mean dip direction of the faults in the seismic reflectivity, matches the mean surrounding GPS extensional direction, suggesting fault displacement is likely to be normal dip-slip. Using a minimum age of 0.51 Ma from nearby sedimentation rates, the measured extension across the 5.4 km length of this study has a rate of 0.19 mm/yr. This is quite a high value for Basin and Range extension and it is likely a result of some influence from the Northern Walker Lane. The lack of an obvious piercing point for shear observed within the seismic volume precludes a clear estimate of strike-slip related motion within the Soda Lake 3D seismic survey. Clear extension and a large fault bend, indicates a localized relay ramp model. With focused extension indicated by two late Quaternary extrusive volcanic bodies, a model of a transtensional pull-apart basin is also considered. Given the few mapped intrabasinal faults at the surface, this

study gives a unique view into fault offsets inside the Carson Sink.

Acknowledgements

I would like to first thank all the people at Magma Energy for access to this wonderful 3D dataset. Jim Echols for helping me to get started understanding the dataset and facilitating the transfer of the survey to UNR. Much thanks to Holly McLachlan, fellow UNR grad student, who worked with me every step of the way and helped keep me informed on all aspects of the resource. Dick Benoit and Frank Monastero for their help and advice on Soda Lake. A thanks also goes out to Dawson Geophysical Company for conducting the survey, and Geokinetics for data processing.

My two advisors, John Louie and Graham Kent deserve a great deal of thanks for their continued support and guidance throughout my studies. I would also like to thank John Louie for writing the grant that allowed me to travel to the University of Auckland to study geothermal well engineering, a highlight of my studies. Bill Hammond merits hearty thanks for all his help on the GPS aspect of this thesis. I also want to thank Wendy Calvin for her help and support at the Great Basin Center for Geothermal Energy through funding from the US Department of Energy. Thanks to my committee members, John Louie, Graham Kent and Alan Fuchs for their time and advice during the reviews of my work. Many thanks also to Lori McClelland and Erik Williams who helped me navigate UNR policies.

Thanks also to the community of students at who helped me with different aspects of this project; Ryan Dingwall, Jayne Bormann, Kyle Gray, Paul Schwering and Alex Morelan. Then there are all the other friends that helped keep me loving life in Reno that are too numerous to list. Finally the greatest thanks to my family who supported me on this entire energy star ride, Dad Robert, Mom Deidre, Sister Alicia.

Contents

List of Figures

Chapter 1   Introduction

This project started when Magma Energy (U.S.) Corporation was chosen for an American Recovery and Reinvestment Act (ARRA) award for the U.S. Dept. of Energy Validation of Innovative Exploration Technologies in the Geothermal Technologies Program. With federal funding of this unproven exploration method the data would need to end up in the hands of the public. James Echols, Holly McLachlan and Richard Benoit helped to familiarize me with this dataset and the geothermal field operations.

The fault and horizon analysis of this seismic data was originally done in highly expensive commercial software, which is not available to the public. My thesis uses an open source and free software (OpendTect®) to do the same analysis with more work on volume manipulation to facilitate better interpretation. The original importation of the dataset into OpendTect® was done by Ryan Dingwall of Southern Methodist University. I then made the fault and horizon interpretations in the software and used these to quantify the fault orientation and horizontal offset.

The GPS aspect of my thesis is a product of MATLAB® scripting written by myself with help from William Hammond. These data were then mapped and analyzed by myself to compare the direction and rate of deformation around the Soda Lake geothermal field.

This paper will be published in *Geosphere* under the themed issue, "Origin of the Sierra Nevada and Walker Lane".

Chapter 2   Journal of Geophysical Research Paper

The following chapter is my submission to *Geosphere* a Geological Society of America publication. I am first author on this paper. My co-authors are: John Louie and Graham Kent of the Nevada Seismological Laboratory, University of Nevada, Reno, Nevada and William Hammond of the Nevada Geodetic Laboratory, University of Nevada, Reno, Nevada.

2.1   Introduction

2.1.1   Geologic and Tectonic Setting

The movement along the North American-Pacific plate boundary is unevenly distributed with approximately half of the deformation being accommodated on the San Andreas fault, although is quite variable depending on the latitude (e.g., greater percentage of motion is accommodated in northern California on the San Andreas fault than southern California) (Wesnousky, 2005b). Dextral shear also occurs along the Walker Lane Deformation Belt and Eastern California Shear Zone (Wernicke, 1992; Atwater and Stock, 1998). This transition zone of the Walker Lane is allowing the northward movement of the Sierran Microplate (Figure 2.1) relative to the Basin and Range Province (Stewart, 1988). According to GPS geodetic studies 20-25% of the plate motion occurs along the Walker Lane in the form of transtensional deformation (Bennet et al., 1998; Faulds et al., 2005; Wesnousky, 2005b; Hammond et al., 2011).

The Northern Walker Lane (NWL) accommodates transtension along the transition of the Basin and Range Province and the Sierra Nevada/Great Valley Microplate on overlapping, left-stepping dextral faults that are being modified due to a young dynamic change in the stress regime (Unruh et al., 2003). One of the sources of this change is from northward migration of the Mendocino triple junction (Faulds et al., 2005). These dextral faults tend to transition to more normal offset and northern strike as they exit the shear of the NWL and enter the extension of the Basin and

Range (Faulds et al., 2005; Wesnousky, 2005a; Wesnousky et al., 2012). Left stepping dextral faults should enable clockwise rotations of fault blocks. Although the majority of fault block rotation in GPS is seen to be slightly counter-clockwise for the NWL (Hammond et al., 2011). Macroscopic Riedel shears are employed as a hypothesis that these stepping-faults are migrating toward the maximum extension in a counter-clockwise development that could account for the GPS block rotation observed (Faulds et al., 2005).

2.1.2 Carson Sink

The Carson Sink trends NE like much of the Basin and Range topography although has a much more equant shape (Figure 2.1). The basin is overlain by Quaternary alluvium, sand dunes, silt and a large playa surface (McNitt, 1990). Like many of the basins in Western Nevada, the Carson Sink exhibits lacustrine deposits that can be attributed to Pleistocene Lake Lahontan (Adams and Wesnousky, 1999; Benson et al., 2002). The NWL tectonic belt borders this area toward the west. Surface faulting indicates basin bounding normal faults (Bell, 1984) and some evidence of strike-slip faulting in the basin (dePolo, 1998; Caskey et al., 2004). The Carson Sink is the surface expression of a complex interaction of shear and extensional forces that cause crustal block rotation (Faulds and Perkins, 2007). It has been proposed that the transfer of NW-trending dextral shear in the Walker Lane to WNW extension in the northern Great Basin would allow for the formation of enhanced extension and pull-apart basins that bring about structural controls for geothermal systems (Faulds and Henry, 2008).

2.1.3 Basin Faulting

Rainbow Mountain fault zone, to the east of the seismic study along the eastern boarder of the Carson Sink (Figure 2.1), demonstrates dextral-normal oblique displacements on east-dipping faults during the most recent Rainbow Mountain-Stillwater earthquake sequence of 1954 (Sawyer, 1999; Caskey et al., 2004). The location of ob-
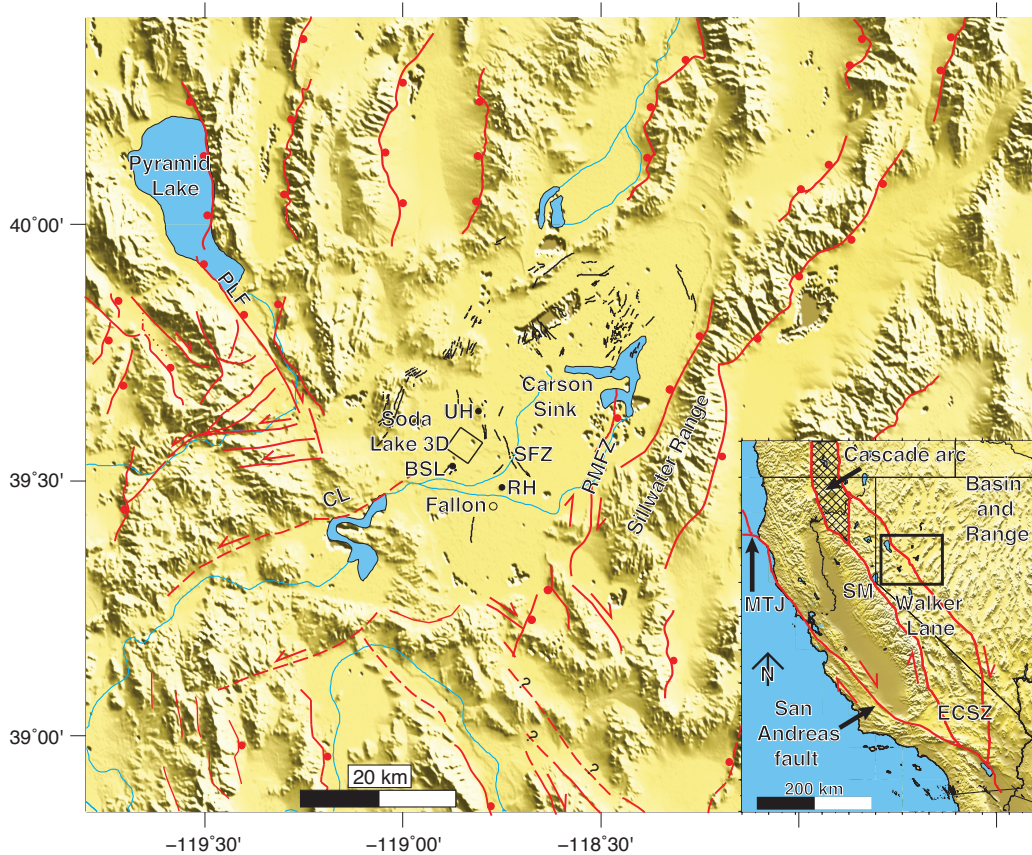
Figure 2.1: Map of the western United States, including major structural trends simplified in red with mapped faults in the Carson Sink in black. Black box indicates the area of the Soda Lake 3D seismic survey. PLF - Pyramid Lake fault; CL - Carson lineament; SFZ - Sagouse fault zone; RMFZ - Rainbow Mountain fault zone; UH - Upsal Hogback; BSL - Big Soda Lake; MTJ - Mendocino triple junction; ECSZ - Eastern California shear zone; SM - Sierran Microplate; RH - Rattlesnake Hill. Modified from U.S.G.S. (2006); Faulds et al. (2005); Caskey et al. (2004); Eisses (2012).

served dextral motion using stream channel offset is at Rainbow Mountain and the Stillwater Point Reservoir. These ruptures extend southwest to the same boundary to the Walker Lane as the Soda Lake 3D seismic survey area (Figure 2.1). The maximum vertical offset at Rainbow Mountain is measured at 0.8 m and the dextral slip has a maximum of 1.0 m (Caskey et al., 2004).

The Carson lineament strikes northeast and its inferred termination is just to the southwest of the Soda Lake 3D seismic survey area (Figure 2.1). This sinistral system of faults offsets Holocene and Pleistocene units and has a low inferred slip-rate of less than 0.2 mm/yr (dePolo, 1998). The fault becomes more broken and discontinuous as it approaches Soda Lake 3D and it is too diffuse to continue into the seismic survey area.

Surrounding the Soda Lake 3D is the Sagouse fault zone, which has the nearest mapped offsets of surficial features (dePolo, 1998). The fault zone offsets late Quaternary volcanic features and Pleistocene Lake Lahontan lacustrine deposits with northeast-to-northwest striking normal faults. A north-south trending horst is interpreted to the northeast of the study and is expressed by two, 3 km long, parallel faults. The Soda Lakes are interpreted to be part of this same fault system that allowed for phreatic subaqueous and subaerial tephra eruptions in the late Quaternary (dePolo, 1998).

2.1.4 Geodetic Setting

The Mobile Array of GPS for Nevada Transtension (MAGNET) network observes surface deformation since 2004 using semi-continuous occupation (Blewitt et al., 2009). This technique places the GPS antenna on fixed steel monument pins that are secured onto stable outcrops that can be run on solar power for months at a time. Then a relatively nearby deployment center utilizes a pool of homogeneous GPS receivers to rotate occupations of each site for, in this case, approximately one month per year (Blewitt et al., 2009). Regional Plate-Boundary Observatory (PBO) GPS stations are continuous and were installed between late 2006 and late 2007.

The velocity vectors used in this study are products of resolving daily GPS solutions (Blewitt, 2008) in alignment with a reference frame rotating with the rigid interior of North America (Hammond et al., 2011). This reference frame, "GB09" uses data through the end of 2009, and isolates the tectonic strain from the GPS coordinate time series. The vectors in this study have also been corrected for post-seismic viscoelastic relaxation due to historic rupture of nearby Stillwater/Rainbow, Dixie Valley, Fairview Peak, Gold King/Louderback faults that ruptured in 1954, the older Cedar Mountain rupture of 1932 and the Pleasant Valley rupture in 1915 (Hammond et al., 2009). In the Carson Sink this post-seismic relaxation signal changes the velocity vectors about 15%.

Profiles across both the Basin and Range and the NWL from Hammond et al. 2011, can provide slip-rates for these two regions to compare to the geodetic and seismic data. One profile across the entire Basin and Range gives an extension rate of ~1 mm/yr over 450 km (Koehler and Wesnousky, 2011). Another closer profile running in the WNW-ESE direction across the Basin and Range provides a ~1 mm/yr velocity change across 250 km (Hammond et al., 2011). Looking across the NWL there is a ~6 mm/yr velocity change across 220 km from the SW-NE (Hammond et al., 2011).

2.1.5   Soda Lake Geothermal Field

The Soda Lake geothermal field is located 10 km (6 mi) northwest of the town of Fallon in Churchill County, Nevada (Figure 2.1). It is in the south-central part of the Carson Sink, which is bordered by the <10,000 year-old Big Soda Lake volcanic explosion crater to the south, and the ~25,000 year-old mafic Quaternary Upsal Hogback volcanic complex to the north (Hill et al., 1979; Sibbett, 1979; Cousens et al., 2012). There are multiple operating geothermal fields within 50 km (30 mi) of Soda Lake (McLachlan et al., 2011).

There are two current power plants, Soda Lake 1 (5.1 MW gross) and Soda Lake 2 (18 MW gross), although they have never reached maximum output. Twenty-

three large diameter wells and six re-drills have been completed, with five used for production and five for injection. This low success rate is due to an inadequate model of the resource, with drilling sites located near the central part of a shallow thermal anomaly (Echols et al., 2011).

The geothermal field was chosen for an American Recovery and Reinvestment Act (ARRA) award for the U.S. Dept. of Energy Validation of Innovative Exploration Technologies in the Geothermal Technologies Program. This provided the funding for the 3D seismic study (Gundy et al., 2010). While most geothermal lithologies in primarily volcanic regions are lacking in clean reflections, this site had a four-line seismic survey done by Chevron in the 1970's that imaged coherent reflections (Echols et al., 2011). These horizontal and expansive reflections of thick sand and mudstone stratigraphy, relatively anomalous in Nevada geothermal systems, made this 3D survey viable at Soda Lake (Echols et al., 2011). At 34 sq km of seismic data, this is one of the largest seismic surveys of any geothermal field to date (Echols et al., 2011).

The seismic volume yielded a detailed map of the fault deformation of the same mudstone horizon found by Chevron, and also defined an inverted-cone-shaped basaltic unit at about 550 m depth (Echols et al., 2011). This extrusive basaltic unit has been dated to about 5.1 Ma (McLachlan and Faulds, 2012). The structural style of this field was interpreted by the operating company to be one of nested pull-apart basins with the thickest sections of basalt in the center of the production area (Echols et al., 2011). Some of the larger fault picks lined up with higher thermal anomalies in wireline data (Echols, pers. comm.).

2.1.6   Mudstone Reflector

A sandstone/mudstone package is the strongest reflector in this survey, appearing from 0.2 to 0.3 seconds two-way travel time, at an approximate depth of 240 m. The interpreted mudstone reflectors illuminate a fault map of recent active tectonics in this basin. This reflective unit consists of shale, mudstone and fine sand that formed

in a deep lacustrine environment (Sibbett, 1979). Assuming an environment of deep lake sediments, this unit was deposited in a paleoplanar orientation. Therefore fault offsets of this unit should demonstrate post-depositional structural deformation of the Soda Lake geothermal field (Echols et al., 2011).

The periodic presence of Lake Lahontan is common in Western Nevada basins for the last ∼1 Ma including Carson Sink, Pyramid Lake to the northwest and Walker Lake to the southwest (Reheis, 1999). Pyramid Lake shows Pleistocene sedimentation rates from sediment cores that indicates that between 47.9 ka and 13.9 ka there was 17.32 m of sediment deposition giving a Pleistocene rate of 0.51 mm/yr (Eisses, 2012). These sediment layers are continuous and show consistent deposition of these reflective units for tens of meters (on the order of >100 ka) past the oldest dates in seismic CHIRP imagery (Eisses, 2012). Walker Lake shows higher sedimentation of 10 m from 13-21 ka, yielding a rate of 1.25 mm/yr (Benson, 1988). These rates are likely overestimations when applied to the more cyclic nature of deposition in the Carson Sink and are used as minimums.

The Rattlesnake Hill basalt, at depth, is about 5 km southeast of the 3D seismic survey (Figure 2.1). This volcanic cone was likely erupted subaerially on the paleosurface of the Carson Sink and ranges in age from 2.5 to 1.03 Ma (Maurer and Welch, 2001). The closest basalt age to Soda Lake that is on the lateral extent of the basalt flow is 1.5 Ma and is ∼30 m below the shallowest indication of the mudstone reflector. Assuming a simple layer cake model for lacustrine sediments, this indicates a maximum age for the mudstone around 1.5 Ma.

2.2   Methods

To estimate the deformation style of the Carson Sink, this study will utilize GPS and 3D seismic survey results. GPS provides a regional look at strain over the last decade, whereas the seismic reflectivity shows a history of deformation spanning hundreds of thousands of years. Examining GPS velocity vectors across the basin can estimate the direction and rate of extension and shear across the basin. 3D seismic imagery allows

for a view at faulted lithology in the basin that has been continually covered with fill and deformed. The deformation observed of this faulted lithology is a product of the strains present since deposition. These two techniques both provide observations of strain but at time scales that are different by ∼4-5 orders of magnitude.

Using the strain values from GPS the two stress regimes of the Basin and Range and Walker Lane can be characterized by comparing the northern and southern ends of the Carson Sink. The results of the quantifiable deformation of faulted units in the 3D seismic study can be compared to the GPS values to help define the forces deforming the geothermal field. Using the direction and rate of deformation this study can compare the influence between the extension of the Basin and Range and the dextral shear of the Walker Lane in this transition zone at the Soda Lake geothermal field.

The goal is to better understand the dynamics of basin deformation and how dextral shear is accommodated in the Carson Sink, then how it relates to Walker Lane and Basin and Range tectonics. Geothermal resources are heavily dependent on the structural regime of fracture patterns for upflow and outflow permeability. This understanding could advance the development of the structural geothermal system model for these types of basins.

2.2.1 GPS

This study utilizes MATLAB® to subtract the regional tectonic deformation, calculate strain tensors and determine a vector and magnitude solution for the deformation of the Soda Lake geothermal field. Forty-six stations are considered for this study, that surround the Carson Sink (Figure 2.2). The stations include 38 that are part of the MAGNET and 8 that are PBO stations. These 46 stations are split into two groups to model the basin deformation of the Carson Sink independent of the larger scale tectonics. The eastern stations defined by a dashed line (Figure 2.2) produce an Euler pole rotational model, after correction for post-seismic motions (about 1mm/yr) due to recent historical earthquakes (Hammond et al., 2009). This analysis was done with

the raw velocity vectors and the results were only about 15% different in most cases. Post-seismic correction mostly reduces the magnitude of the extension in the basin and range because of the proximity to recent ruptures. This Euler pole rotational model is then extrapolated to estimate vector solutions of the western stations. The difference between the modeled Euler pole vectors and the "GB09" velocity vectors indicate the direction of localized basin deformation relative to the eastern Stillwater Range. Tensor solutions for the northern and southern region are shown in green and purple respectably, produced by the same color stations (Figure 2.2). The Soda Lake 3D seismic survey is between these two groups of tensor solutions.

At the 3D seismic survey an averaged velocity vector and tensor solution provide an estimation of the modern deformation. Stations within 30 km are considered, which allows for 12 stations, and these are weighted based on proximity to the seismic study for the velocity vector (Figure 2.2). The weighting provides that stations at 10 km be twice as influential as stations at 20 km. The tensor solution for the seismic survey uses the same stations for the calculation, without weighting the station vectors.

The simplest way to find a rate of extension across the geothermal field is from the tensor solution. If all of the extension is being accommodated on faults that are perpendicular to the direction of maximum extension then the tensor solution yields the horizontal offset in nanostrain/yr. This is calculated by dividing the horizontal offset over a given time period by the horizontal distance producing the unitless ratio of strain over the time in years.

2.2.2 3D Seismic Survey

The 3D (and three-component) reflection seismic survey occupies an area of 34 sq km (13 sq mi) with 8,374 source points and 3001 receivers. There are 52 paired source lines with a pair separation of 33.5 m (110 ft). Source interval is 33.5 m (110 ft) and the paired, northeast-trending source lines are separated by 235 m (770 ft). Receivers are spaced at 67 m (220 ft) on 36 northwest-trending lines separated by 168
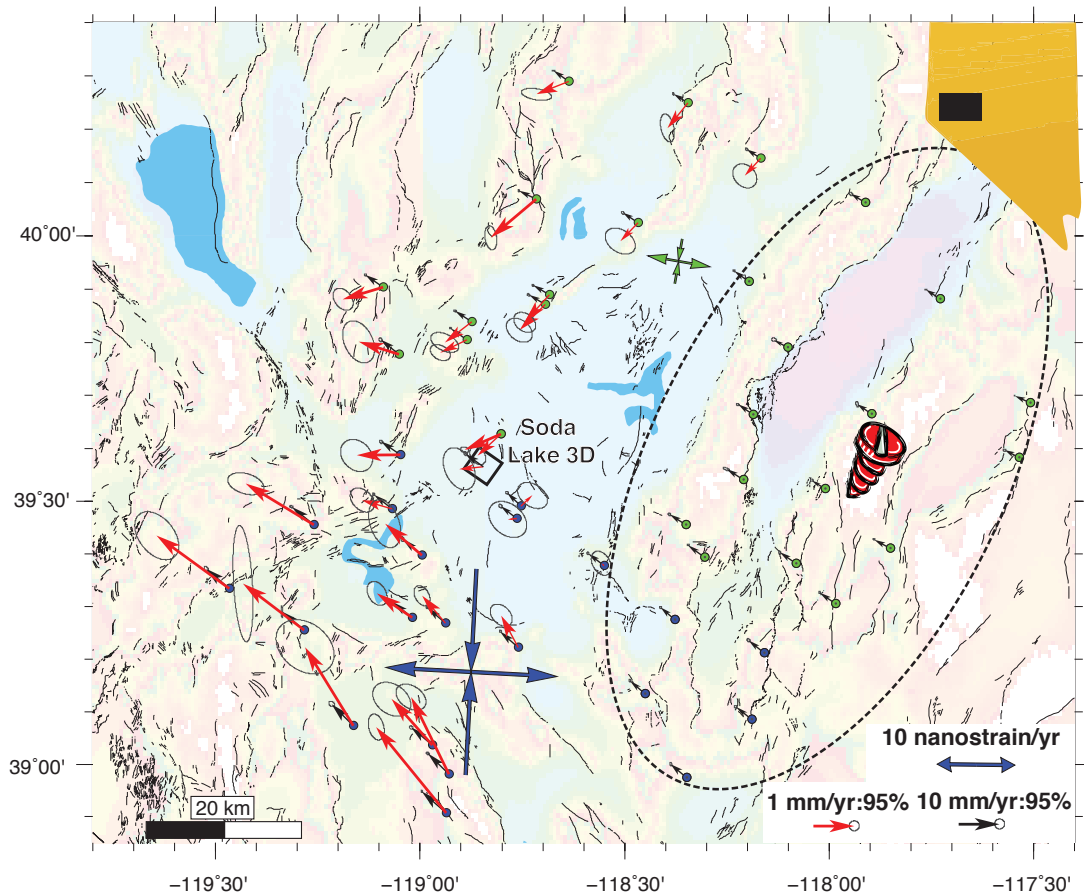
Figure 2.2: Black vectors are with respect to a rigid North America, "GB09", and corrected for post-seismic motions. The screw is meant to symbolize how the stations within the dashed line are in the Euler pole rotational model, which is held stable to produce the differenced deformation represented by the red vectors across the Carson Sink. The purple stations produce the purple tensor solution in the south and the green stations produce the green tensor solution in the north.

m (550 ft). This design provides 17 m (55 ft) common midpoint (CMP) bins with high fold (40) in the 600 by 1200 m (2000 ft by 4000 ft) area of original interest. The mudstone under investigation here is shallower and therefore has a potential lower fold. This geometry was originally planned for just single component geophones, but during project approval it was upgraded to include three-component recording. However, due to the long permitting process already underway the geometry of the survey could not be changed. The source is alternating sets of three 28,000 kg (62,000 lb) vibroseis trucks undertaking two sixteen-second-long, 8-72 Hz sweeps per source point.

This survey's P-wave data were processed first by a field static correction, and then a model-based noise attenuation to eliminate low-velocity surface-wave noise. Two passes of stacking velocity analysis with a 0.8 km (0.5 mile) interval and surface-consistent residual statics were done. A curved-ray 3D Kirchhoff prestack time migration (PSTM) provided velocity analysis. Another curved-ray 3D Kirchhoff PSTM approach with sufficient half-aperture, 75-degree migration dip, including P-wave VTI-anisotropy (if significant) and PSTM residual velocity analysis, yielded the final image volume. The velocity model applied to convert the PSTM to prestack depth migration (PSDM) (Figures 2.3A and 2.4A) is relatively simple and horizontally continuous for the shallow section at and above the mudstone although accounts for the faster velocities and lateral heterogeneity at the basaltic unit (Echols et al., 2011).

We interpreted the seismic volume in OpendTect®. Multiple steps were taken according to specialized workflows to facilitate the interpretation of faults and horizons in this volume. First, a dip-steered volume was produced to allow for the following processing of attributes to steer according to the structural dip of the reflections. A median filter applied to the volume reduced noise spikes and preserved reflection trends. Similarity attributes calculated located reflection offset in the volume to get a non-interpreted fault map along the Z-plane (Figure 2.5) (Chopra and Marfurt, 2007). To give a sharper contrast at the faults, reflector amplitudes were migrated toward areas of lower similarity using a diffusion filter (Figures 2.3B and 2.4B). Using

this fault-enhanced volume assisted the interpretation of the surface of the mudstone horizon and the faults that offset reflectors above and below the unit.

2.3 Data Analysis

2.3.1 GPS

The black arrows on Figure 2.2 represent the total velocity field with respect to a stable North American Plate, and the stations with red arrows outside the dashed ellipse show the localized deformation along the Carson Sink. The residual velocity vectors (red) are relative to a stable Stillwater range to the east and exhibit a changing deformation field from the southwest to the northeast. In the southwest corner, the vectors show the fastest relative deformation toward the northwest. The magnitude of the regional velocity vectors decrease toward the Soda Lake 3D study area and have a relatively constant magnitude southwest of that, and also further to the northeast. The direction of the relative station movement transitions from toward the northwest to more southwest for the stations in the northern part of the Carson Sink. The green stations on Figure 2.2 show a strain tensor for the northern stations that has more extension than compression, and lower magnitudes of strain. The purple stations in the south allow for a strain tensor that is more compression than extension, and shows higher magnitudes of strain.

At the Soda Lake 3D site the weighted average velocity vector shows motion in the southwest direction (Figure 2.2). The tensor solution for the Soda Lake 3D site (Figure 2.6) appears to be an amalgamation of the two tensor solutions for the stations to the north and south. Intermediate tensor solutions that move along this transition from the southwest to the northeast show a gradual transition of strain amplitude and direction. The Soda Lake 3D site rates are comparable to the southern sites and the orientation is similar to the solution for the northern sites.
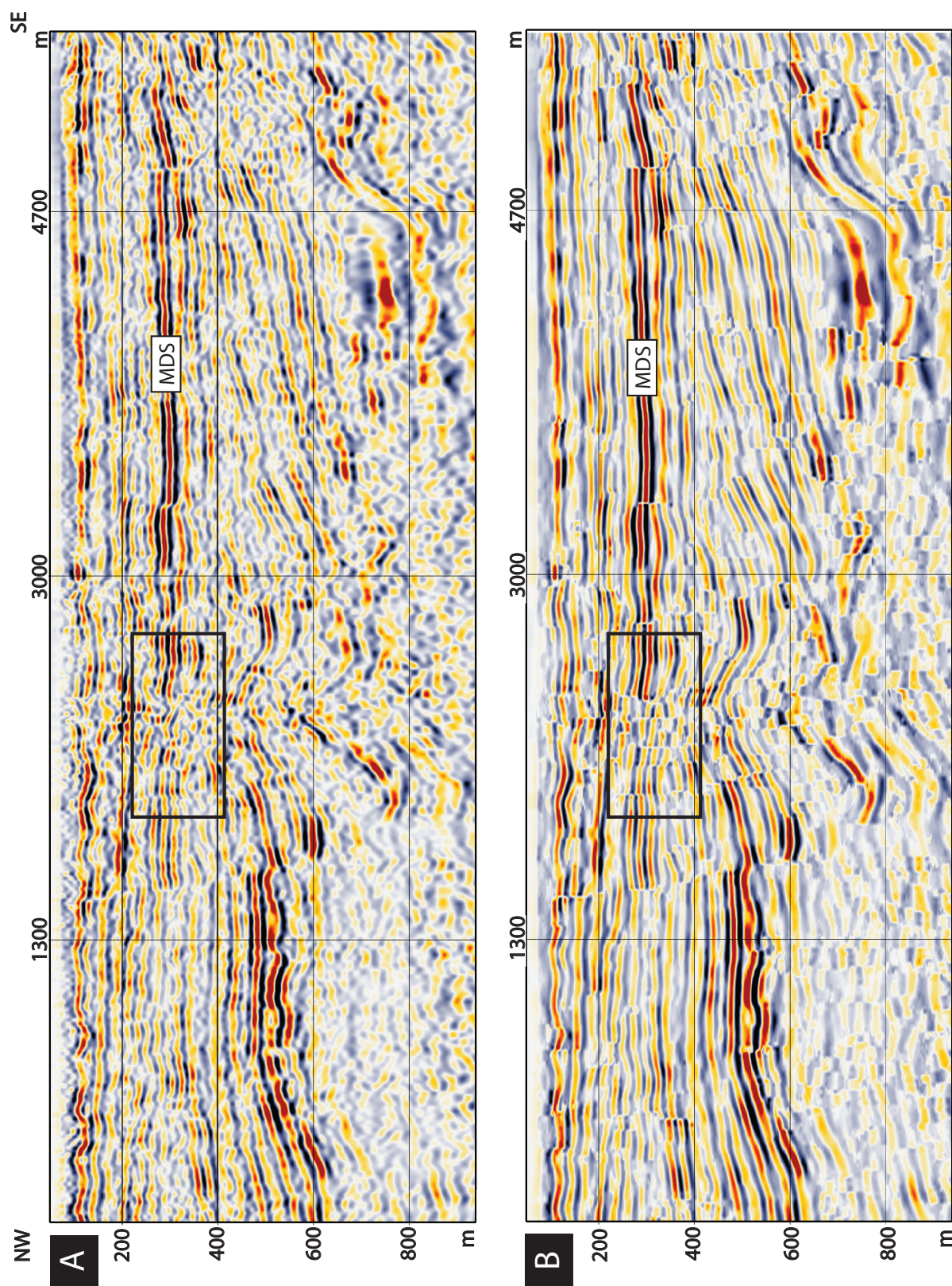
Figure 2.3: Cross-sections along inline 76 show the pre-stack depth migration (A) and the fault enhanced volume (B). The mudstone is indicated (MDS) and the upper strong positive (blue) reflection is the most coherent horizon. The box indicates an area of the survey that is greatly improved by the volume processing and allows for better fault recognition. Vertical exaggeration is 5 times.
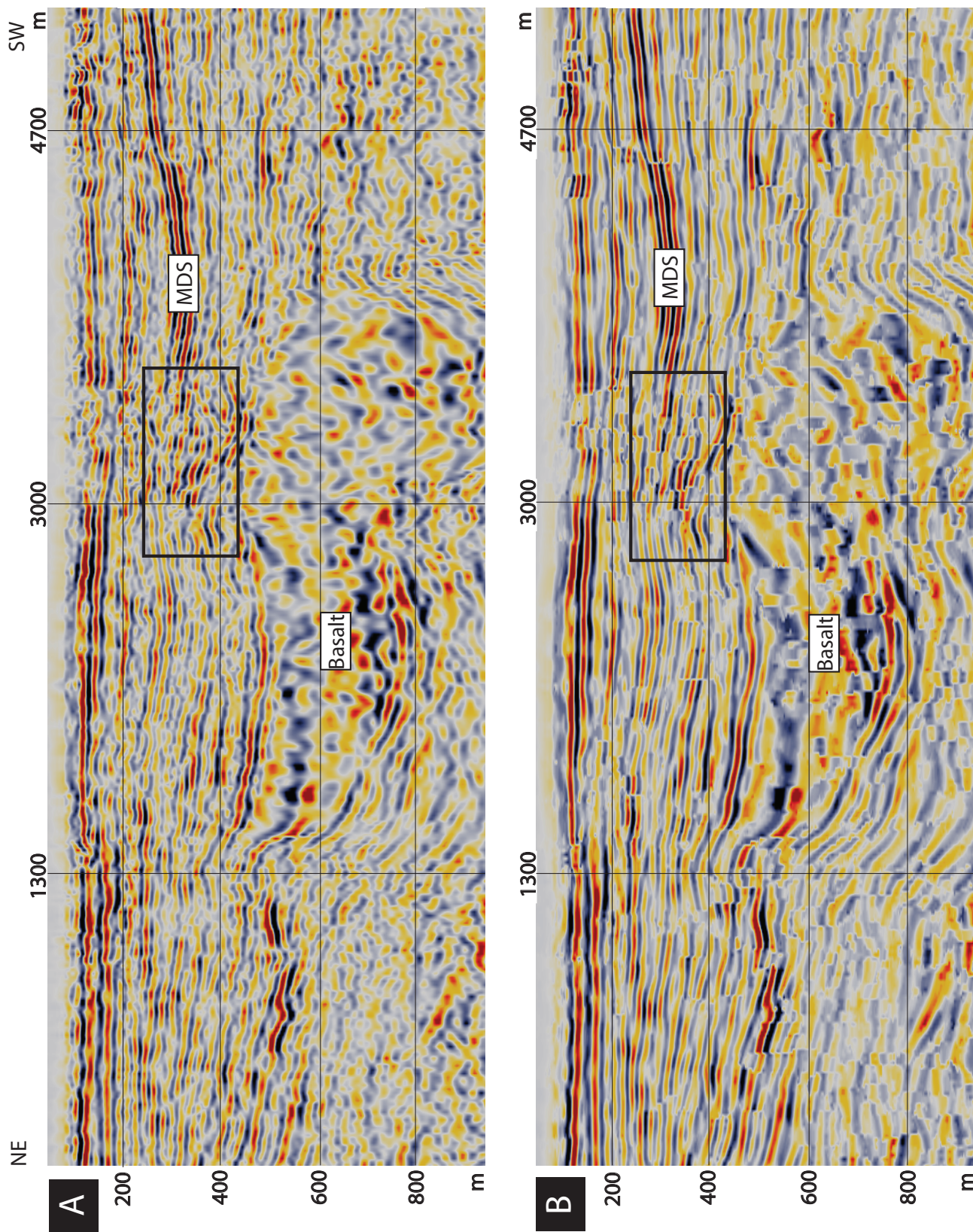
Figure 2.4: Cross-sections along crossline 295 show the pre-stack depth migration (A) and the fault enhanced volume (B). The mudstone (MDS) and basalt are indicated. The upper strong positive (blue) reflection is the most coherent horizon. The box indicates an area of the survey that is greatly improved by the volume processing and allows for better fault recognition. Vertical exaggeration is 5 times.
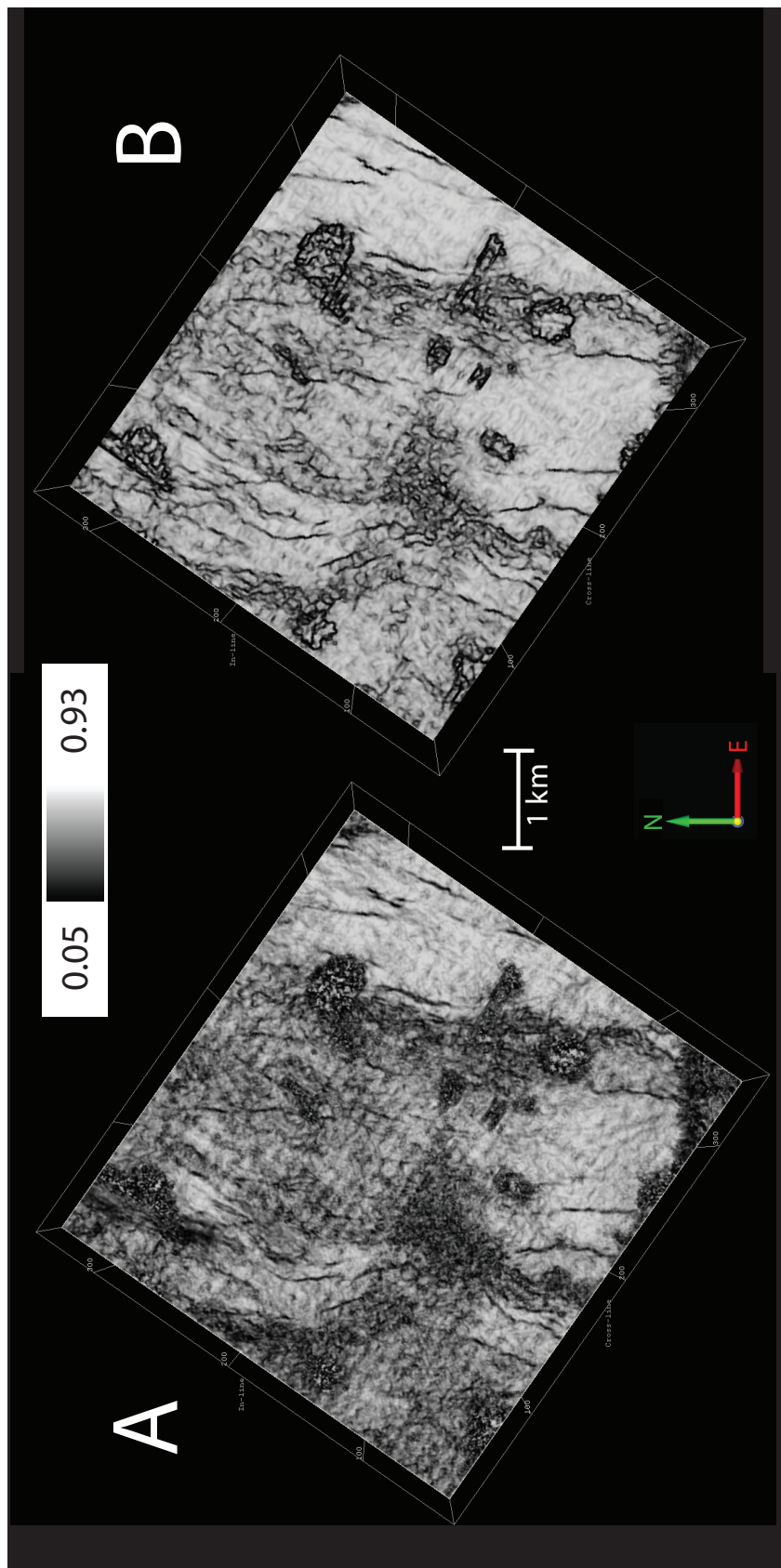
Figure 2.5: This map view shows the seismic survey at a depth of 290m from the surface. The attribute displayed looks at the similarity of adjacent waveforms with higher similarity closer to 1. The similarity of the raw volume is on the left (A) and the similarity of the fault-enhanced seismic is shown on the right (B). This product gives an uninterpreted view of faults (strike N-S) through the seismic survey.
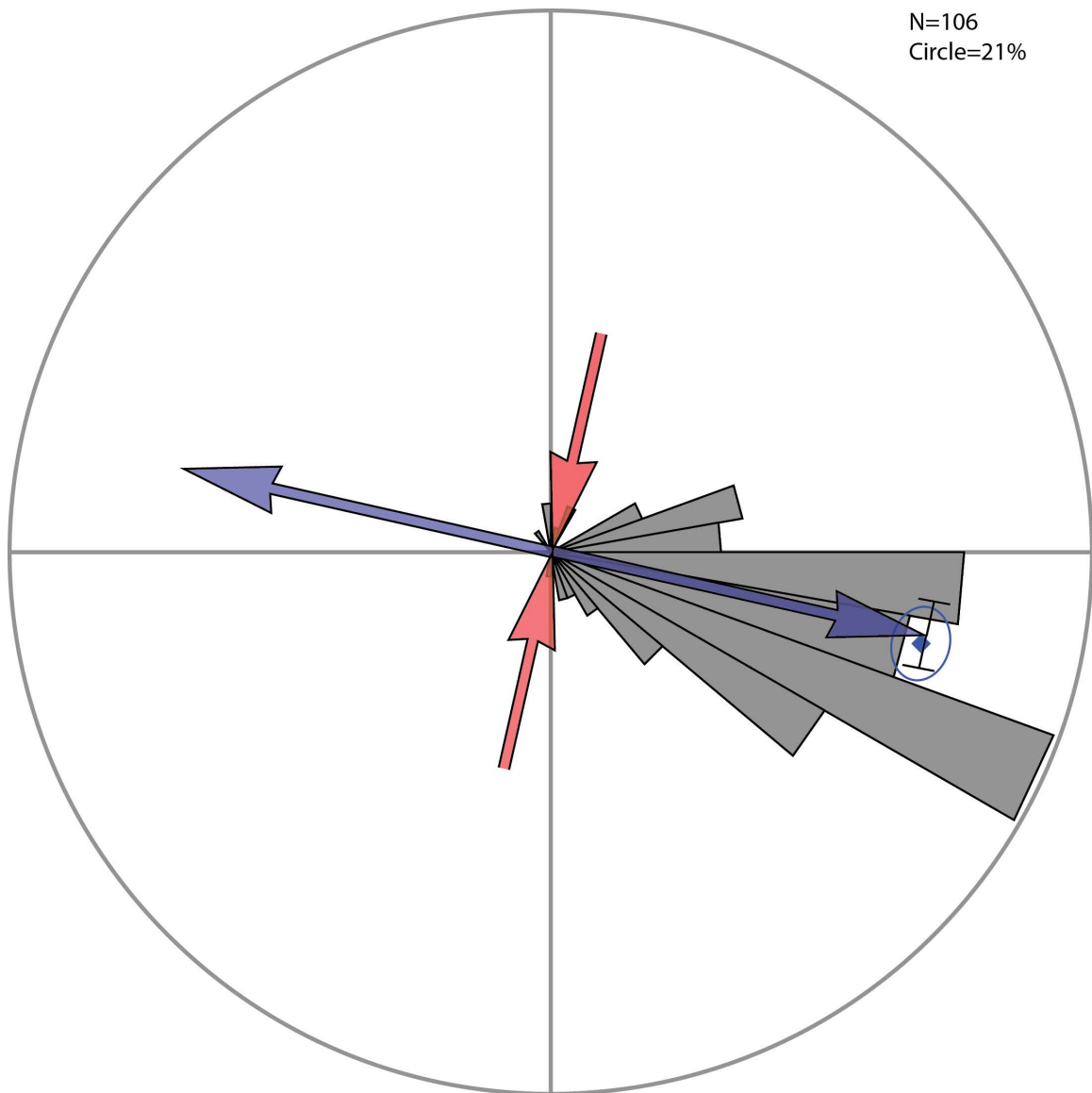
Figure 2.6: The grey wedges in this rose diagram are the dip directions of the 106 faults picked in the study. The edge of the circle is 21% of the total fault dips for the seismic. The blue diamond and blue oval symbolize the mean (102°) and the 95% confidence ellipse of that mean. The red and blue arrows represent the tensor solution for the GPS stations in a 30 km radius around Soda Lake 3D to estimate strain for the field. The bracket shows the error for the azimuth of extension.

2.3.2 3D Seismic Survey

Faults and horizons picked in the 3D seismic provide interpreted structural offsets of the paleoplanar mudstone in the seismic volume. To facilitate the picking of faults the "similarity" seismic attribute volume in horizontal, constant-depth section recognizes the recent fault pattern cutting the mudstone (Figures 2.5 and 2.7). This map view shows the general strike of the faults and the nature of their discontinuities. The majority of picked fault planes strike between north and northeast with some antithetic faults in the central part of the survey (Figure 2.8). The fault patterns show en-echelon fault steps, large left bends and some antithetic-striking faults.

Fault picks were made on the inline vertical sections of the fault-enhanced seismic volume because it is closer to perpendicular to the general fault strike. The fault picks were then checked on the crossline vertical sections. The faults are assumed to be planar and have normal displacement. A minimum of 6 m of vertical offset in the mudstone is nominally required to delineate any fault because 6 m is a quarter of the wavelength of the dominant frequency ($\sim$70 Hz) of the mudstone reflector. The best-picked faults cut both deeper features, and the mudstone by more than 6 m (#1 in Figure 2.9). Less well-observed faults cut the mudstone but less clearly offset the lower stratigraphy (#2 in Figure 2.9). Faults that offset both the mudstone and lower units are picked until all units are continuous again. This can result in fault picks that have little to no mudstone offset in certain cross-sections (#3 in Figure 2.9). Often in this survey the lower units have larger offset along the fault plane than the mudstone. There are also discontinuities that are artifacts of the fault enhancement process that are not picked as faults (#4 in Figure 2.9).

To analyze the dip direction of the faults a simplified fault map is prepared, to estimate the strike of over one hundred faults. The calculation of the extensional direction involves the assumption that all north to northeast striking faults have an eastern dip (Figure 2.6). This avoids the bimodal distribution of the same extension directions from horst and graben features that have parallel strikes but oppositely dipping fault planes. The rose diagram (Figure 2.6) shows a mean fault dip trending
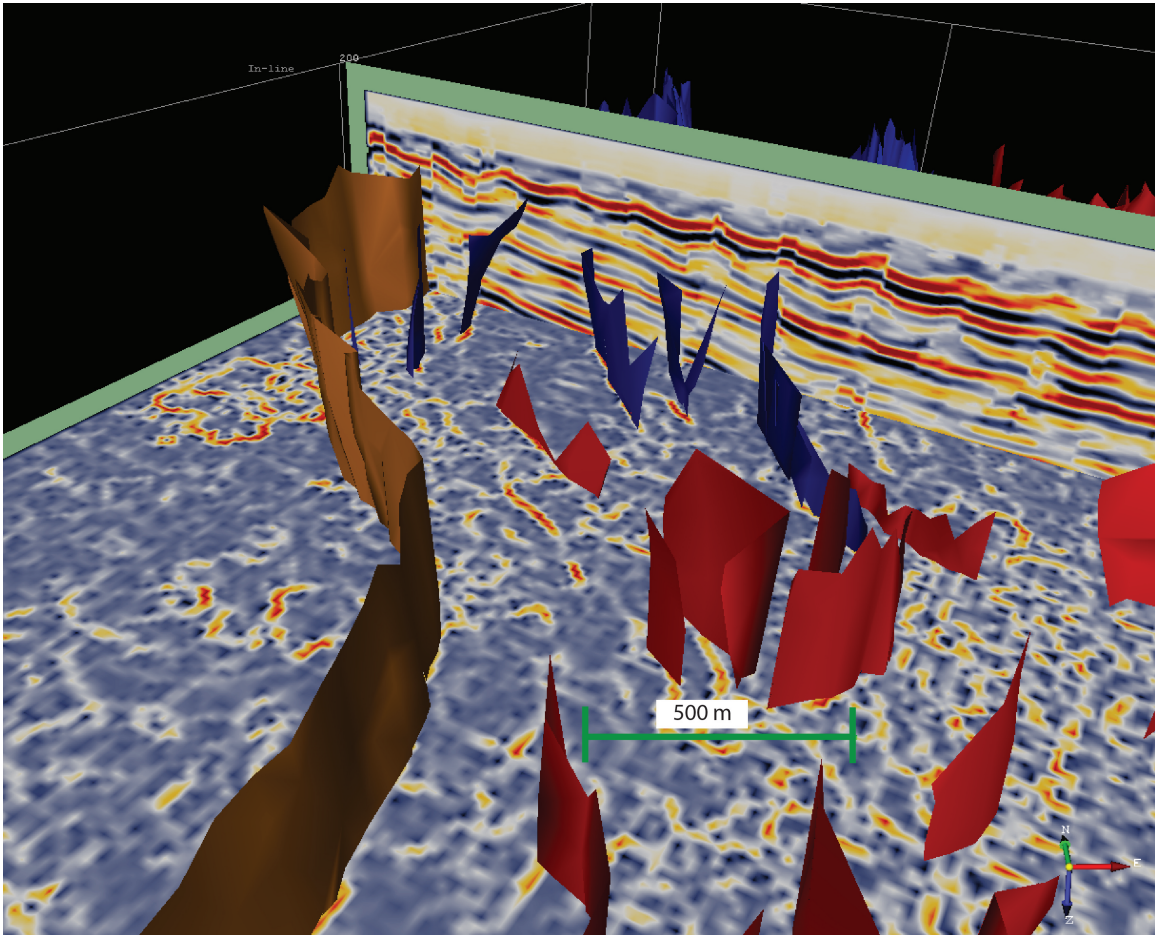
Figure 2.7: The fault planes are sticking out of a z-plane of similarity that shows zones of lower similarity along fault planes. Not all of the low similarity lines have faults because they may not have been continuous enough to offset the shallower mudstone. The cross section shows the fault-enhanced seismic volume. Vertical exaggeration is 5 times.
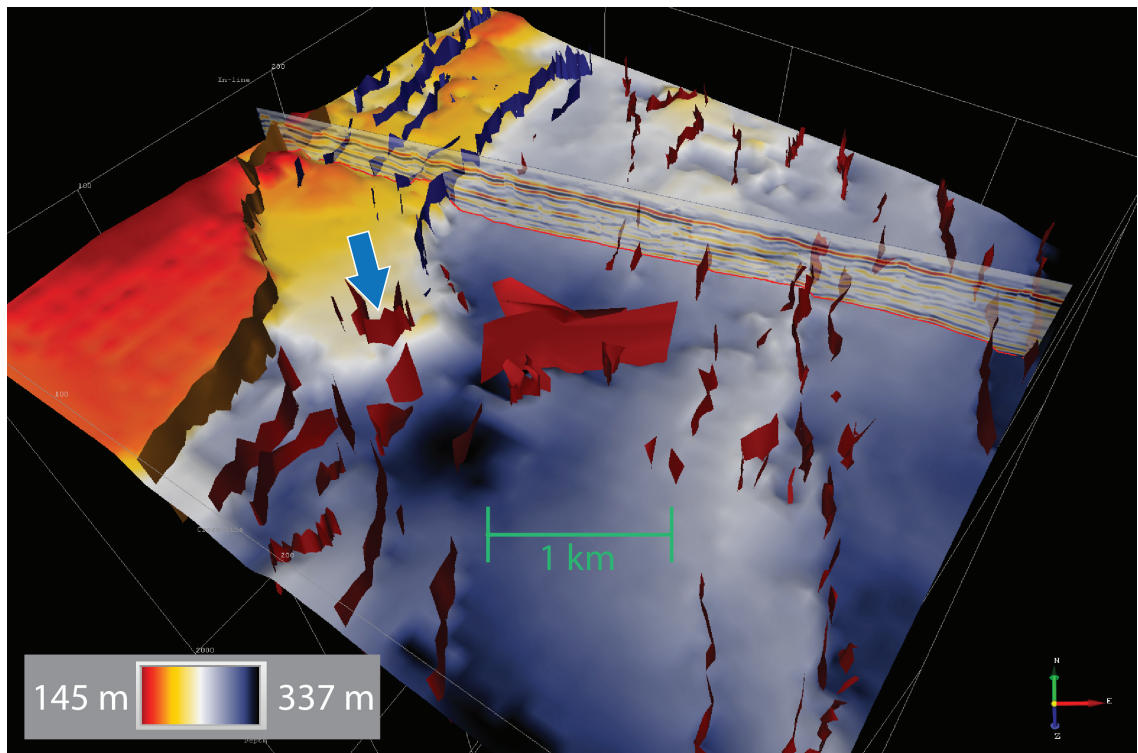
Figure 2.8: An oblique view of the mudstone horizon topography with fault picks shown. The geothermal production and relative mudstone low is south of the east-striking faults. The structural ramp is shown on the west side of the image sloping down toward the viewer from a red high to a blue low. The relative ridge is along the east side. Transparent cross-section is the same as Figure 2.9. The arrow indicates the ramp, between two major faults, that leads toward the highly faulted accommodation zone. Color on the fault planes is used just to differentiate zones of faulting across the field. Color bar indicates depth to mudstone. Vertical exaggeration is 5 times.

102° with an ellipse for the 95% confidence of that mean.

The vertical offset and dip of the faults are calculated along a cross section located perpendicular to faulting (Figure 2.9). There are 13 faults across this line with 8 dipping east and 5 dipping west. The average dip of these faults is 66° with a total length of the cross section being 5.4 km. If the horizontal offset of all the faults is individually totaled, the offset is calculated at 96 m across 5.4 km. Assuming that this is a paleoplanar lacustrine mudstone then we can use this as a value for extension across the survey, a cumulative extensional strain of 1.8%.

The mudstone unit is expressed as a source waveform of large amplitude in the clearest areas of the seismic survey (Figure 2.3 and 2.4). The choice to tie the mudstone horizon to the first maximum positive seismic amplitude reflection arises from the overall coherence of that feature throughout the survey area. In some areas this maximum positive becomes the only high-amplitude reflection to follow (#5 in Figure 2.9). The gamma ray logs in four wells, also indicated that this reflector had the broadest peak in radioactivity, indicating a more consistent and thicker fine-grained lithology. Using the well logs and cores to tie this horizon to depth, the deformation in this unit can yield direct evidence of strain during the Pleistocene or possibly even the Pliocene, depending on the uncertain age of this unit, perhaps somewhere between the extremes of 0.5 to 1.5 Ma.

Topography of the mudstone unit shows a relative low near the bend of the faults that coincides with where peak geothermal production is located (Figure 2.8). Along the east side of the survey there is an interpreted horst or half-graben structural feature that creates a ridge in the mudstone horizon striking north-south. There is a ramp between the two major faults on the west-side of the study that slopes down to the south. The horizon is at a mean depth of 255 m and a minimum of 150 m.
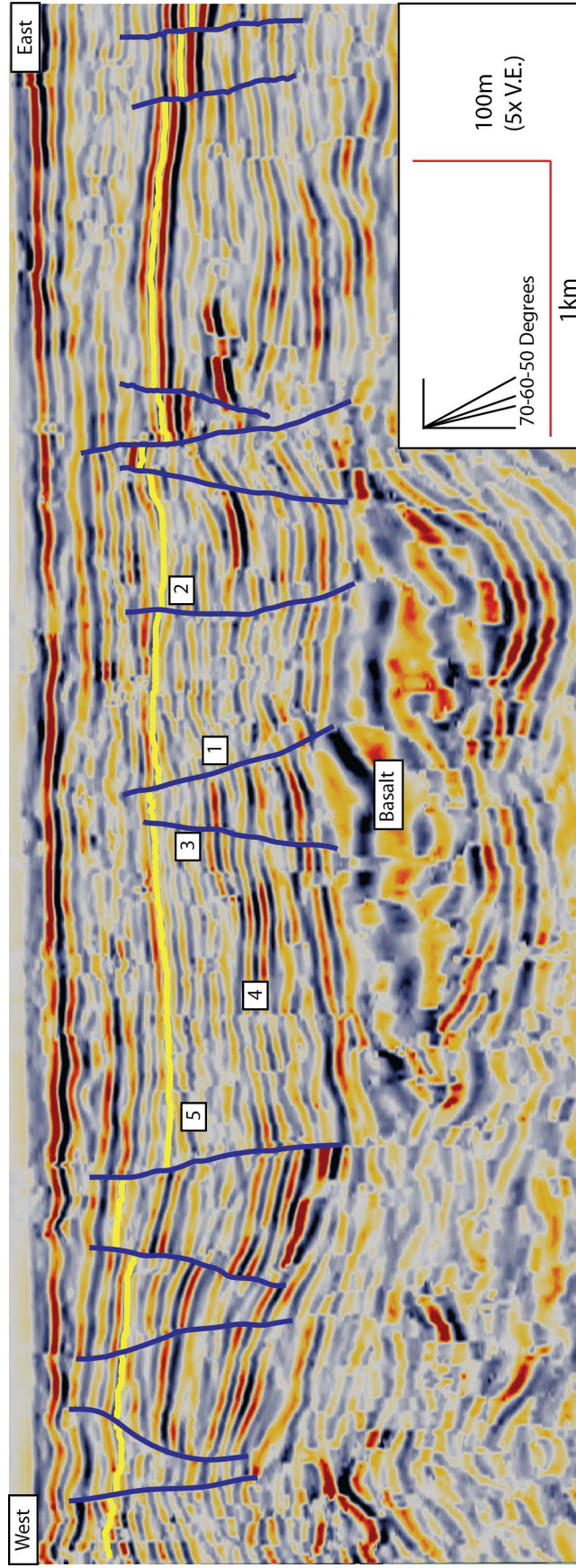
Figure 2.9: This fault-enhanced inline vertical section demonstrates the variety of fault picks with horst and graben features across the study. The 5.1 Ma basaltic unit is indicated by the high amplitude and long wavelength reflections.

2.4   Interpretations

2.4.1   GPS

In the GPS deformation dataset there is a transition between two structural regimes across the Carson Sink. The stations in purple (Figure 2.2) in the southwest of the basin show shear as the velocity vector magnitudes decrease toward the Soda Lake 3D. When the general fault strike toward the northwest and the tensor solution showing maximum compression and extension are combined the result is preferential dextral shear across these faults in the Walker Lane. The green stations in the northeast show a different style of deformation with faults striking northeast and the tensor solution showing a larger ratio of extension, which is perpendicular to fault strike. This deformation regime favors normal displacement along the faults in the Great Basin. The Carson Sink is roughly wedge-shaped, and the velocity vectors show a difference in relative direction that could account for this shape. The north end of the Carson Sink vectors are oblique to the main basin while in the southern section the vectors are more directly parallel to the longest section of the basin.

At the location of the Soda Lake geothermal field and seismic study the vector average and tensor solution more closely resemble the deformation of the Great Basin in terms of orientation. The tensor solution has elements of both structural patterns because it needs a number of surrounding stations to calculate a strain field. Averaging over all stations within 30 km of the Soda Lake 3D survey area makes the tensor solution more diffuse. Strain is most likely high with a value of maximum extension at 30.4 nanostrain/yr due to the Walker Lane influence (Figure 2.6). If this strain value is assumed to have been consistent since the deposition of the mudstone, then it would take 580 ka $\pm$ 76 ka to accumulate the offset indicated in the seismic cross section (Figure 2.9).

2.4.2   3D Seismic Survey

The temporal setting of the paleoplanar mudstone is uncertain. The extrusive basalt at 600 m depth provides an absolute maximum age of 5.1 Ma and the basalt at Rattlesnake Hill provides an interpreted maximum age of 1.5 Ma. Assuming a sedimentation rate similar to Pyramid Lake at 0.51 mm/yr (Eisses, 2012), the mean depth to the mudstone horizon (255 m) would indicate an age of 500 ka. If the minimum depth (150 m) is used this would yield an age of 294 ka. Although using the minimum depth does not factor in preferential deposition in relative topographical lows. Assuming that the mean depth yields a minimum age of the mudstone the extension of 96 m gives a maximum extension rate of 0.19 mm/yr. This rate would be even higher if the age of 294 ka was used. Using the inferred maximum age (1.5 Ma) of the mudstone the rate is 0.064 mm/yr. A rate of 0.19 mm/yr is almost a fifth of the extension across a nearby GPS profile extending 250 km of the Basin and Range (Hammond et al., 2011), all in just 5.4 km. The minimum rate of 0.064/yr is still three times larger (for 5.4 km) than the average Basin and Range strain in the same GPS profile. This seems unreasonable; either this age is far too young or extension related to the NWL is enhancing this estimate near the Soda Lake 3D survey area.

The structural map from the depth of the mudstone horizon (Figure 2.8) shows a ramp leading to a relative low point. With no piercing point, there is no way to infer the amount of strike slip motion for these faults. The GPS and 3D seismic show good evidence for pure extension in the localized area of the geothermal field, and if the system was purely extensional, it would be interpreted as a step-over or relay ramp in a normal fault zone (Larsen, 1988; Faulds et al., 2005), although the 3D seismic survey lacks a major fault to connect the offset to the south (Figure 2.8).

A pull-apart basin is another interpretation that would allow for partitioning of normal and strike-slip motion (Wu et al., 2009; Brothers et al., 2009; Gürbüz, 2010; Mann et al., 1983). This would account for the consistent east-dipping faults and the step-over with pure extensional displacement in the Soda Lake 3D. For this hypothesis to be valid there also needs to be dextral-slip motion orientated 120 ° from

the extensional faults. This dextral motion would be striking 134° compared to the 14° strike of the mean fault direction in the study. This orientation coincides with NWL tectonics surficially shown by faults along the southern boundary of the Carson Sink and the Sagouse fault zone to the northeast of the seismic study (Figure 2.1). Although there is a lack of a NWL oriented fault to the northwest of the 3D seismic to connect possible strike-slip offset. Pull-apart basins also tend to focus extension (Wu et al., 2009), which could account for the specific points of recent volcanism expressed on the surface by Big Soda Lake and the Upsal Hogback.

2.5 Acknowledgements

Chapter 3   Conclusions

Using both GPS and 3D seismic a two-stage representation of the deformation in the Carson Sink, Nevada allows for multiple structural hypotheses to explain localized extension and crustal thinning. GPS provides a view of enhanced extension in comparison to Basin and Range tectonics. If used as an average deformation rate for the Soda Lake 3D seismic survey area, this approach yields a similar age to the minimum age derived from sedimentation rates. A fault and horizon map of the Soda Lake 3D is produced and quantified to correlate the two periods of deformation. Two indicators of deformation separated by about half a million years or more, show the same direction of deformation. It is possible that there has been little directional change to tectonics in this region recently. Then there are two factors that indicate that this system is undergoing higher deformation than expected from the surrounding slow Basin and Range tectonics. The seismic volume demonstrates evidence for comparatively large amounts of offset, in comparison to Basin and Range expectations. The tensor solution also provides a similar solution to the Basin and Range but with larger values of strain, indicating some influence from the Northern Walker Lane. The two interpretations of either a step-over or pull-apart system are presented and there is no slip evidence to disprove either.

3.1   Additional Work

This study provides a framework that could benefit greatly from some additional study of the Carson Sink. The first aspect is the absolute or relative dating of the mudstone unit. Relative dating could be achieved through a better correlation to the Rattlesnake Hill basalt to the southeast that has a date of 1-2 Ma (Maurer and Welch, 2001). There are 2D seismic lines that were shot there and if these two studies were connected with another 2D line this would help give a better bound to this deformed mudstone unit. More seismic lines or 3D studies to the north or the south could

investigate the possibility of dextral slip accommodation on Northern Walker Lane oriented faults.

To further investigate the deformation of the Carson Sink the GPS network could be expanded to include a semi-continuous site at Big Soda Lake, which would help to better surround the geothermal site. As time passes the velocity vectors and their error values will become more stable and later evaluation of these signals will have the benefit of better-constrained data.

Appendix A   Responsibility Agreement

I understand that I am responsible for follow-up, revisions, etc. of the preceding paper upon submittal to *Geosphere*, a Geological Society of America publication. I agree to include co-authors on revisions and to ask them for clarification on anything I am uncertain about.

Bibliography

Adams, K. D., and S. G. Wesnousky, 1999, The lake lahontan highstand: age, surficial characteristics, soil development, and regional shoreline correlation: Geomorphology, **30**, 357–392.

Atwater, T., and J. Stock, 1998, Pacific–north america plate tectonics of the neogene southwestern united states: An update: International Geology Review, **40**.

Bell, J. W., 1984, Quaternary fault map of nevada, reno: Scale 1:250,000, Nevada Bureau of Mines and Geology Map 79.

Bennet, R. A., B. Wernicke, and J. Davis, 1998, Continuous gps measurements of contemporary deformation across the northern basin-range province: Geophysical Research Letters, **25**, 563–566.

Benson, L., 1988, Preliminary paleolimnologic data for the walker lake subbasin, california and nevada: Water-Resources Investigations Report 87-4258, U.S. Geological Survey.

Benson, L., M. Kashgarian, R. Rye, S. Lund, F. Paillet, J. Smoot, C. Kester, S. Mensing, D. Meko, and S. Lindstrom, 2002, Holocene multidecadal and multi-centennial droughts affecting northern california and nevada: Quaternary Science Reviews, **21**, 659–682.

Blewitt, G., 2008, Fixedpoint theorems of gps carrier phase ambiguity resolution and their application to massive network processing: Ambizap: J. Geophys. Res., **113**.

Blewitt, G., W. C. Hammond, and C. Kreemer, 2009, Geodetic constraints on contemporary deformation in the northern walker lane: 1. semi-permanent gps strategy, *in* Late Cenozoic Structure and Evolution of the Great Basin–Sierra Nevada Transition: Spec. Pap. Geol. Soc. Am., **447**, 1–15.

Brothers, D. S., N. Driscoll, G. M. Kent, A. J. Harding, J. M. Babcock, and R. L. Baskin, 2009, Tectonic evolution of the salton sea inferred from seismic reflection data: Nature Geoscience, **2**, 581–584.

Caskey, S. J., J. W. Bell, A. R. Ramelli, and S. G. Wesnousky, 2004, Historic surface faulting and paleoseismicity in the area of the 1954 rainbow mountain–stillwater earthquake sequence, central nevada: Bulletin of the Seismological Society of America, **94**, 1255–1275.

Chopra, S., and K. Marfurt, 2007, Seismic attributes for prospect identification and reservoir characterization: Society of Exploration Geophysicists. SEG Geophysical Developments Series, No. 11.

Cousens, B., C. D. Henry, and V. Gupta, 2012, Distinct mantle sources for pliocene–quaternary volcanism beneath the modern sierra nevada and adjacent great basin, northern california and western nevada, usa: Geosphere, **8**, 562–580.

dePolo, C., 1998, A reconnaissance technique for estimating the slip rate of normal-slip faults in the great basin, and application to faults in nevada, u.s.a. University of Nevada, Reno unpublished Ph.D. dissertation.

Echols, J., D. Benoit, M. Ohren, G. Oppliger, and T. V. Gundy, 2011, Integration of a 3d-3c reflection seismic survey over a known geothermal resource: Soda lake, churchill county, nevada: Transactions, Geothermal Resources Council, 1633–1641.

Eisses, A., 2012, New constraints on slip-rates, recurrence intervals, and strain partitioning beneath pyramid lake, nevada: Master's thesis, University of Nevada, Reno.

Faulds, J. E., and C. D. Henry, 2008, Tectonic influences on the spatial and temporal evolution of the walker lane: An incipient transform fault along the evolving pacific-north american plate boundary, *in* Ores and Orogenesis: Circum-Pacific tectonics, geologic evolution, and ore deposits: Arizona Geological Society Digest, **22**, 437–470.

Faulds, J. E., C. D. Henry, and N. H. Hinz, 2005, Kinematics of the northern walker lane: An incipient transform fault along the pacific–north american plate boundary: Geological Society of America, **33**, 505–508.

Faulds, J. E., and M. E. Perkins, 2007, Evidence for dextral shear along the western margin of the carson sink; the missing link between the central and northern walker lane, western nevada: Abstracts with Programs, Geological Society of America, 15–15.

Gundy, T. V., G. Oppliger, M. Ohren, D. Benoit, and M. Morrisson, 2010, Utilizing a comprehensive 3d model to understand, maintain, and expand the soda lake geothermal resource, nevada usa: Transactions, Geothermal Resources Council, 1185–1189.

Gürbüz, A., 2010, Geometric characteristics of pull-apart basins: Lithosphere, **2**, 199–206.

Hammond, W. C., G. Blewitt, and C. Kreemer, 2011, Block modeling of crustal deformation of the northern walker lane and basin and range from gps velocities: Journal of Geophysical Research, **116**, 1–28.

Hammond, W. C., C. Kreemer, and G. Blewitt, 2009, Geodetic constraints on contemporary deformation in the northern walker lane: 3. central nevada seismic belt postseismic relaxation, *in* Late Cenozoic Structure and Evolution of the Great Basin–Sierra Nevada Transition: Spec. Pap. Geol. Soc. Am., **447**, 21.

Hill, D. G., E. Layman, C. M. Swift, and S. H. Yungul, 1979, Soda lake, nevada, thermal anomaly: Presented at the Transactions, Geothermal Resources Council.

Koehler, R. D., and S. G. Wesnousky, 2011, Late pleistocene regional extension rate derived from earthquake geology of late quaternary faults across the great basin, nevada, between 38.5 °n and 40 °n latitude: GSA Bulletin, **123**, 631–650.

Larsen, P. H., 1988, Relay structures in a lower permian basement-involved extensional system, east greenland: Journal of Structural Geology, **10**, 3–8.

Mann, P., M. R. Hempton, D. C. Bradley, and K. Burke, 1983, Development of pull-apart basins: Journal of Geology, **91**, 529–554.

Maurer, D. K., and A. H. Welch, 2001, Hydrogeology and geochemistry of the fallon basalt and adjacent aquifers, and potential sources of basalt recharge, in churchill county, nevada: Water-Resources Investigations Report 01-4130, U.S. Geological Survey.

McLachlan, H. S., W. R. Benoit, and J. E. Faulds, 2011, Structural framework of the soda lake geothermal area, churchill county, nevada: Transactions, Geothermal Resources Council, 925–930.

McLachlan, H. S., and J. E. Faulds, 2012, Some new constraints on the stratigraphic and structural setting of the soda lake geothermal field, churchill county, nevada: Presented at the American Geophysical Union Transactions.

McNitt, J. R., 1990, Stratigraphic and structural controls of the occurrence of thermal fluid at the soda lake geothermal field, nevada: Geothermal Resources Council Transactions, **14**.

Reheis, M., 1999, Highest pluvial-lake shorelines and pleistocene climate of the western great basin: Quaternary Research, **52**, 196–205.

Sawyer, T.L., c., 1999, Fault number 1679, rainbow mountain fault zone,: in Quaternary fault and fold database of the United States: U.S. Geological Survey website, http://earthquakes.usgs.gov/hazards/qfaults, **accessed 02/25/2013 10:45 AM.**

Sibbett, B. S., 1979, Geology of the soda lake geothermal area: Master's thesis, University of Utah Research Institute.

Unruh, J., J. Humphrey, and A. Barron, 2003, Transtensional model for the sierra nevada frontal fault system, eastern california: Geology, **31**, 327–330.

U.S.G.S., 2006, Quaternary fault and fold database for the united states: from USGS web site: http//earthquakes.usgs.gov/regional/qfaults/, **accessed 02/25/2013 10:45 AM**.

Wernicke, B., 1992, Cenozoic extensional tectonics of the u.s. cordillera, *in* The Cordilleran orogen: Conterminous U.S.: Boulder, Colorado, Geological Society of America, Geology of North America, **G-3**, 553–581.

Wesnousky, S. G., 2005a, Active faulting in the walker lane: Tectonics, **24**, 1–35.

———, 2005b, The san andreas and walker lane fault systems, western north america: transpression, transtension, cumulative slip and the structural evolution of a major transform plate boundary: Journal of Structural Geology, **27**, 1505–1512.

Wesnousky, S. G., J. M. Bormann, C. Kreemer, W. C. Hammond, and J. N. Brune, 2012, Neotectonics, geodesy, and seismic hazard in the northern walker lane of western north america: Thirty kilometers of crustal shear and no strike-slip?: Earth and Planetary Science Letters, **329**, 133–140.

Wu, J. E., K. McClay, P. Whitehouse, and T. Dooley, 2009, 4d analogue modelling of transtensional pull-apart basins: Marine and Petroleum Geology, **26**, 1608–1623.